Tensegrity Lander Architectures for Planetary Explorations

Dipanjan Saha[1], Raman Goyal[2] and Robert E. Skelton[3]

[1]Postdoctoral Researcher, Department of Aerospace Engineering, Texas A&M University, TX, USA; email: dipanjan1989@tamu.edu
[2]Graduate Student, Department of Aerospace Engineering, Texas A&M University, TX, USA; email: ramaniitrgoyal92@tamu.edu
[3]TEES Distinguished Research Professor, Department of Aerospace Engineering, Texas A&M University, TX, USA; email: bobskelton@tamu.edu

ABSTRACT

This paper investigates two different tensegrity topologies with a few adjustable structure parameters as candidate planetary landers. The overarching goal is to seek the minimal mass designs that can keep the acceleration of a payload below a specified value during landing after a free fall. It is required that the payload stays above the ground, or in the worst case, just touches the ground with zero velocity. It is also required that no tensile member yields, and no compressive member either buckles or yields during impact. The topologies investigated in this study are the tensegrity prism and the double-helix tensegrity (DHT). In particular, this study considers a square prism and a four-legged DHT with additional string-to-string networks. The complexity of the structure in the vertical direction, prestress, and damping coefficient of each tensile member are treated as design variables for both prism and DHT. Simulating tensegrity dynamics in terms of node and connectivity matrices, a trade study is presented to compare payload accelerations for the two architectures with variable complexity, prestress, and damping. Candidate minimal mass designs are obtained by reducing bar diameters iteratively till all the bars and strings remain intact. Results presented in the paper demonstrate that the prism landers have a clear advantage over the DHT landers in terms of mass and acceleration. The two-stage tensegrity prism requires the smallest mass of all the architectures considered in this work.

INTRODUCTION

Tensegrity systems refer to a network of axially-loaded members, such that each member belongs to one of two groups, where the first group consists of elastic members called *strings* which can only be in tension, and the second group consists of rigid members called *bars* which can only be in compression (Skelton and de Oliveira 2009; Fuller et al. 1975). Tensegrity systems are becoming popular to construct engineering structures such as bridges, towers, domes, and so on (Carpentieri et al. 2015; Bel Hadj Ali 2010; Tibert and Pellegrino 2003) because of various advantages. It was shown in the literature that tensegrity leads to the minimal mass solutions under five different types of loading: compressive, tensile, simply supported, cantilever and torsional (Skelton and de Oliveira 2009;

Skelton and de Oliveira 2010a; Skelton and de Oliveira 2010b). Although no individual member experiences any bending moment, the overall system can still bend due to the coupled motion of bars and strings (Karnan et al. 2017; Paul et al. 2006; Bel Hadj Ali 2010). The absence of bending moments indicates that the deforming force in each member is only in one direction, and this leads to reliable high-precision mathematical models. Using node and connectivity matrices, the dynamics of tensegrity systems of *any* complexity was described in (Goyal and Skelton 2019). Furthermore, in contrast to the traditional approach of designing the structure first and then designing the controller to obtain the required performance, tensegrity provides a framework to simultaneously select the structure and controller parameters for the desired control objective. The integration of structure and control designs leads to more efficient use of control energy. This also allows engineers to make a decision on whether active control is needed or not. The precision of sensors and actuators needed to accomplish the control objective can also be simultaneously solved (Li et al. 2008; Goyal and Skelton 2019).

Saving material cost by virtue of minimal mass designs as well as the potential to absorb energy in the strings makes tensegrity a good candidate for the design of impact structures. A very relevant example of an impact structure is a spacecraft lander. A lander often carries a payload, which typically contains the electronics needed for planetary explorations. The dynamic behavior of the system during impact with the ground evolves on a significantly fast time-scale, and it is a challenging problem to design the structure such that the payload is protected during the impact (SunSpiral et al. 2013). An approach using bent buckled beams was presented in the work of (Rimoli 2016) to design tensegrity landers. Keeping the same topology for the lander, a subsequent work (Goyal et al. 2019b) showed that the mass of the structure can be reduced, while the energy absorption can be increased by replacing the beams with tensegrity D-bars (Skelton and de Oliveira 2009) of suitable complexity.

While the authors' previous work (Goyal et al. 2019b) established the promise of using tensegrity topologies for lander design, a few issues related specifically to the *dynamics* of the structure during impact are yet to be investigated. Although the previous work accounts for a given static load, it is of great importance that the acceleration of the payload remains within a specified bound at all times as the structure hits the ground after a free fall. It also needs to be ensured that there is no yielding or buckling of the members as the structure makes contact with the ground. In addition, the previous work studied a specific tensegrity topology. Using another topology, it may be possible to reduce the peak acceleration of the payload. Furthermore, within a given topology, it is possible to influence the payload acceleration in multiple ways. For a given height and footprint of the lander, the *complexity* - defined here as the number of stages in the vertical direction - dictates the angle at which the bars hit the ground. The static equilibrium for a tensegrity structure has an infinite number of solutions for

the force density in each string, known as the *prestress*. By choosing different prestresses, it is possible to make the structure softer or stiffer. Each string in a tensegrity structure has some stiffness and some damping. Therefore, within a given tensegrity topology, the payload acceleration can be affected by choosing suitable complexity, prestress, and damping in each string.

This paper studies the effect of complexity, prestress, and string damping on the peak acceleration of the payload for a total of five lander architectures made out of two different tensegrity topologies: the tensegrity prism, and the double helix tensegrity (DHT) (Nagase and Skelton 2014). Subsequently, an attempt is made to find out candidate minimal mass designs for all the architectures. The structure is assumed to land after free fall on a lunar environment, with the lunar soil characterized by stiffness and damping coefficients. Using a recently developed MATLAB-based software to simulate the dynamics of tensegrity structures (Goyal et al. 2019a), a range of values of prestress and damping is established for each architecture such that the peak acceleration of the payload is within a specified bound within this range. Reducing bar diameters iteratively until the point of failure, candidate minimal mass designs are produced for every architecture.

This paper is organized in the following sections. The next few sections discuss the architectures and the parameters used for numerical simulations. Simulation results showing peak acceleration of the payload and candidate minimal mass designs are discussed in the subsequent section. The final section describes conclusions and future work.

TENSEGRITY LANDER ARCHITECTURES USED FOR THE CURRENT STUDY

In the literature, tensegrity structures of both class-1 and class-K were modeled by a system of highly coupled nonlinear differential equations (Goyal and Skelton 2019) involving the node matrix, the bar connectivity matrix and the string connectivity matrix. Landing on a lunar environment is simulated in MATLAB for several cases of nonlinear class-1 and class-K dynamics in the current work (Goyal et al. 2019a). The architectures simulated in the current study are constructed by making relevant modifications to two well-known tensegrity topologies.

Tensegrity Prism

A discussion on regular tensegrity prisms can be found in (Skelton and de Oliveira 2009). The top and the bottom contain the same number of nodes. The prism can maintain self-equilibrium if the top face is oriented at a certain angle with respect to the bottom face. The angle depends on the number of nodes at the top or the bottom. In order to add some safety against toppling upon landing, the current work considers square prisms. For a square prism to maintain static equilibrium, the top square is oriented at 45 degrees with respect to the bottom.

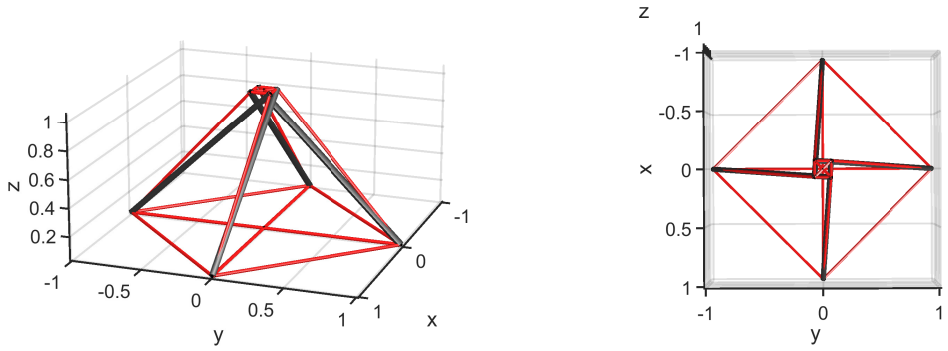

(a) **Perspective view** (b) **Top view**

Figure 1: **Single-stage prism lander (all dimensions in meters)**

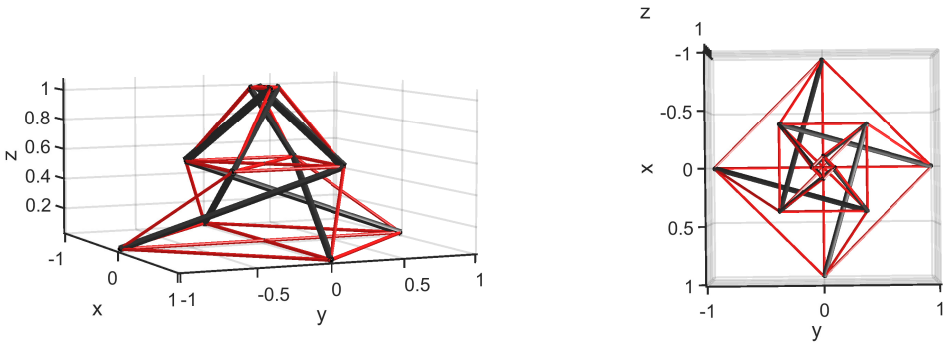

(a) **Perspective view** (b) **Top view**

Figure 2: **Two-stage prism lander (all dimensions in meters)**

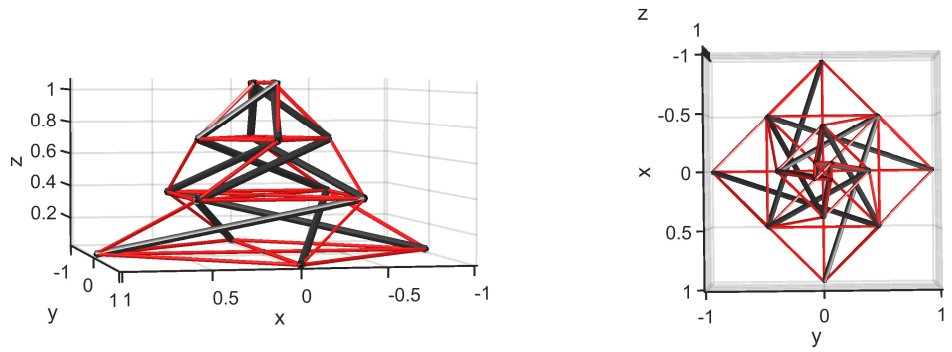

(a) **Perspective view** (b) **Top view**

Figure 3: **Three-stage prism lander (all dimensions in meters)**

In order to examine the effect of complexity, the current work studies single-stage, two-stage, and three-stage tensegrity prisms. For multi-stage architectures, one stage is placed on top of another, thereby increasing complexity in the vertical direction. For each stage, the top square is oriented at 45 degrees relative to the

bottom. For consecutive stages, the rotations of the top squares relative to the bottom are in the same direction. To reduce the impact during vertical landing, it is beneficial to absorb energy in the horizontal direction. Keeping this in mind, an additional string-to-string network is inserted such that four strings connect to the center of each square from its endpoints. This leads to additional string-to-string nodes in the structure, and the payload is placed at the topmost string-to-string node such that it has the maximum possible separation from the ground upon landing. Figures 1 - 3 show the single-stage, two-stage and three-stage prism architectures respectively. The red lines represent the strings, and the black lines represent the bars. It is to be noted that the single-stage prism is a class-1 structure. The two-stage and three-stage prisms are constructed such that at most two bars can touch at every node; hence they are class-2 structures.

Double Helix Tensegrity (DHT)

A discussion on DHTs can be found in (Nagase and Skelton 2014). In this topology, a sequence of bars goes along the circumference of the structure in the counter-clockwise sense, while another sequence of bars goes along the circumference in the clockwise sense.

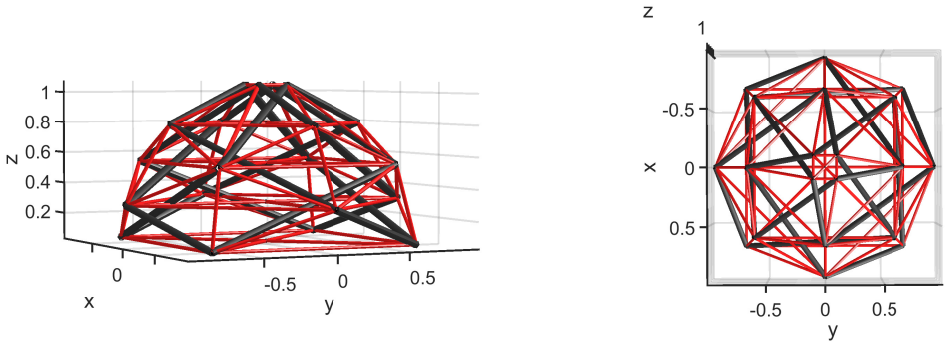

(a) **Perspective view** (b) **Top view**

Figure 4: **Two-stage DHT lander (all dimensions in meters)**

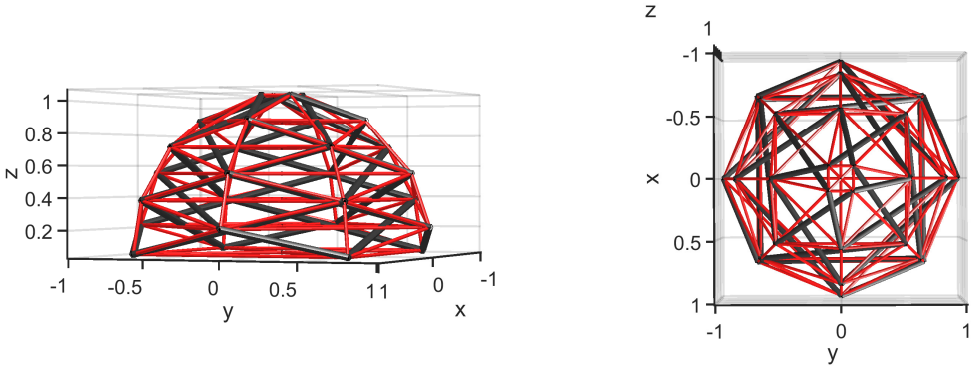

(a) **Perspective view** (b) **Top view**

Figure 5: **Three-stage DHT lander (all dimensions in meters)**

The complexity of a DHT is characterized by two positive integers p and q, where p represents the number of nodes on a horizontal plane, and q represents the number of self-similar vertical stages. For comparison with the prism, p is assumed to be four, i.e. the structure is assumed to land on four legs. In this case, two sets of squares can be found along horizontal cross-sections. One set of squares is oriented at 45 degrees relative to the other set for the structure to retain self-equilibrium. Two cases of vertical complexity q are studied: $q = 2$ and $q = 3$. In order to absorb energy in the direction orthogonal to that of the impact and prevent the structure from folding inside out upon landing, an additional string-to-string network is inserted. At each level of four horizontal nodes forming a square, four strings are added from each node to the center of the square. The payload is placed at the center of the topmost square. Figures 4 - 5 show the two-stage and three-stage DHT architectures respectively. Both architectures are examples of class-2 tensegrity structures.

FIXED PARAMETERS IN THE CURRENT STUDY

For a fair comparison, some parameters are assumed the same for all of the numerical simulations conducted in this study.

Lunar Soil Characteristics

The lunar soil is assumed to have a stiffness of 10^6 N/m and a damping constant of 10^3 N-s/m. These data are in accordance with (Sutton and Duennebier 1970).

Gravity

For simulating landing on the moon, the lunar gravity is assumed to be 1.6 m/s^2. The accelerations are evaluated as multiples of earth-gravity $g = 9.8$ m/s^2.

Height and Footprint of the Structure

For all the architectures, the height of the structure is assumed to be 1 m, and the footprint, i.e., the length of a diagonal of the bottom square is assumed to be 2 m. Two extremes of the selections of height and footprint are as follows. If the footprint is too small and the height is too large, the structure is likely to topple. On the other hand, if the footprint is too large and the height is too small, the payload at the top is likely to hit the ground. The numbers for the height and footprint are selected to remain in the middle of the two extremes.

The general idea is to increase the width of the stages from top to bottom in order to avoid toppling. The diagonal of the highest square is one-tenth that of the lowest. For the prisms, the width of the stages changes linearly with height. On the other hand, each DHT architecture is a hemisphere.

Properties of the Structural Members and Payload

All the bars are assumed to be of carbon fiber with a density of 1400 kg/m^3, Young's modulus of 2.3×10^{11} Pa and yield stress of 3.5×10^9 Pa. All the strings are assumed to be of Ultra-High Molecular Weight Poly-Ethylene (UHMWPE) with a density of 970 kg/m^3, Young's modulus of 1.2×10^{11} Pa and yield stress of

2.7×10^9 Pa. For simulation, the payload is assumed to be a point mass of 1 kg, placed at the center of the topmost square.

It is to be noted that in general, bars contribute to the mass of a tensegrity structure significantly greater than strings. Therefore, the bar diameters are varied to influence the structure mass, whereas the string diameters are kept constant. The simulations are conducted in two steps, and the bar diameters are constant at 8 cm in the first step. Variation of bar diameters in the second step is discussed in the next subsection. The diameter of each string is fixed at 5 mm. The numbers 5 mm for string diameter and 8 cm for bar diameter are chosen after some trial and error such that no string yields and no bar buckles or yields for a sufficiently large range of prestress and damping.

The dimensions and architecture of the structure fix the stiffness of each string as $k_s = \frac{E_s A_s}{l_s}$, where E_s is the Young's modulus, A_s is the cross-sectional area and l_s is the string length. Moreover, the Euler buckling load for each bar is $F_b = \frac{\pi^3 E_b (\frac{d_b}{2})^4}{4 l_b^2}$ where E_b is the Young's modulus, d_b is the bar diameter, and l_b is bar length.

Initial Conditions

To capture the dynamic behavior of landing after a free fall, the initial conditions are set such that all the nodes have an initial velocity of 30 cm/s, and the bottom of the structure is at 5 cm from the ground at time zero. The current study assumes that the structure falls vertically before it makes contact with the ground. Initially, the structure is at self-equilibrium, and gravity is the only external force acting downward. As a result, the structure makes contact with the ground 0.125 seconds into the simulation at a downward velocity of 50 cm/s.

Integration Time-Step

After some trial and error, it is found that an integration time-step of 0.1 ms adequately captures the dynamics of the tensegrity system during the impact.

VARIABLE PARAMETERS IN THE CURRENT STUDY

In addition to complexity discussed in the section on lander architectures, three other variables used in the study are prestress, string damping, and bar diameter.

Prestress

Tensegrity systems can be in static equilibrium with an infinite number of solutions for the force densities in the strings. In the current simulation, the minimum allowable value of the force density in any string is taken as an input. This fixes the force densities in all the strings, and will henceforth be referred to as the *prestress parameter*, denoted as $\bar{\gamma}$. The current study considers large variations of the prestress parameter, $\bar{\gamma} \in [10^{-3}, 10^3]$ N/m, and examines the effect on the peak acceleration of the payload as the structure goes from softer to stiffer.

String Damping

Realistically, the damping in the elastic strings should be small. It is desirable to keep the damping ratio $\zeta \leq 0.1$. Depending on the other parameters of all the strings, if the damping coefficient for every string is chosen to be $c = 1000$ N-s/m, the maximum of all the string damping ratios is equal to 0.06, which is close to 0.1. Moreover, the damping ratio is linearly proportional to the damping coefficient. The damping coefficient c of each string varies from 1 N-s/m (i.e. almost zero damping) to 1000 N-s/m (i.e. reasonable damping) for the current study.

Bar Diameter

The diameter of every bar is fixed at 8 cm in the first step. In the second step, the bar diameters are progressively reduced by half until any of the members fail by either yielding or buckling.

RESULTS

A recently developed MATLAB-based software simulated the dynamics of the architectures shown in Figures 1 - 5, as they land on a lunar environment. The payload carries electronic instruments that are expected to survive accelerations up to $20g$, where g is the earth gravity. To add a reasonable margin of safety, the *preferred* upper bound on peak payload acceleration is fixed at $10g$. The simulations are carried out in two steps. The objective of the first step is to find out the range of damping and prestress to keep acceleration within $10g$, when the bar diameters are fixed at 8 cm. The second step is to keep reducing bar diameters to find out the candidate minimal mass design for each architecture.

Step I: Fixed Bar Diameter; Varying Prestress and Damping

For different values of string damping coefficients c and prestress parameters $\bar{\gamma}$, peak accelerations of the payload are plotted in Figures 6 - 8.

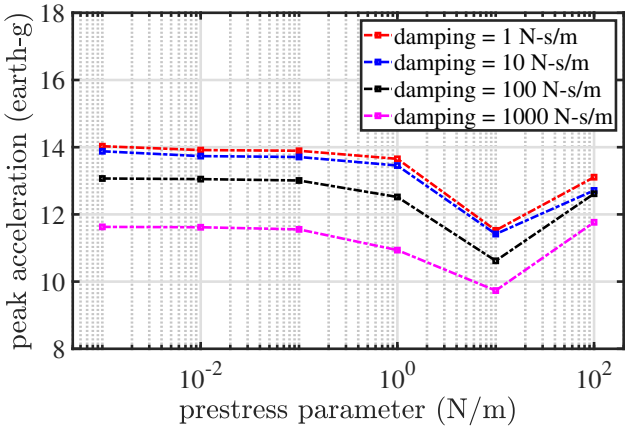

Figure 6: **Payload acceleration vs. prestress for different values of string damping for the single-stage prism**

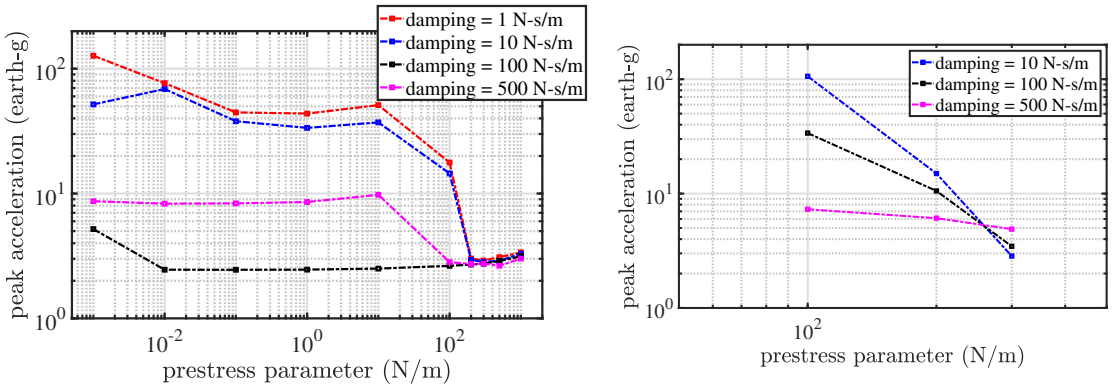

(a) **Two-stage prism** (b) **Three stage prism**

Figure 7: **Payload acceleration vs. prestress for different values of string damping for multi-stage prisms**

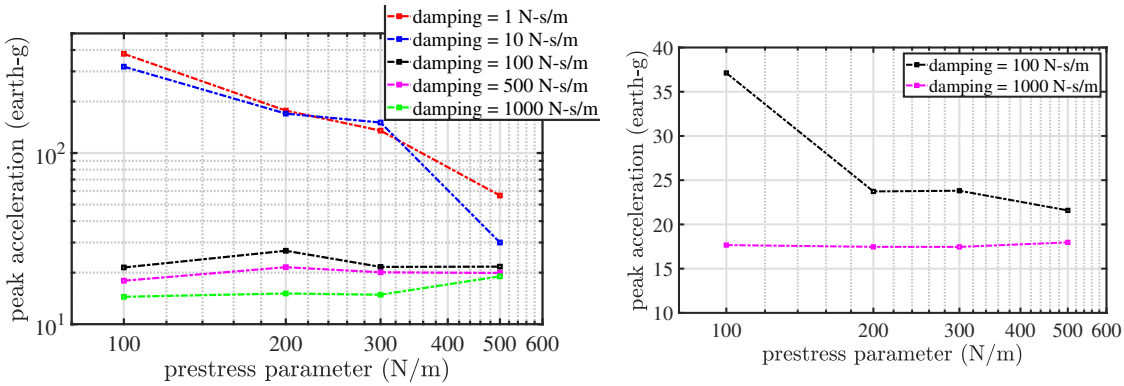

(a) **Two-stage DHT** (b) **Three-Stage DHT**

Figure 8: **Payload acceleration vs. prestress for different values of string damping for two-stage and three-stage DHTs**

Since it is easier to alter prestress simply by choosing a different initial length of a string, prestress is plotted along the X-axis of each figure, while damping is shown parametrically. Figure 6 shows that the combination of $\bar{\gamma} = 10$ N/m and $c = 1000$ N-s/m achieves a peak acceleration of less than $10g$ for a single stress prism. For other combinations of damping and prestress, the peak acceleration is higher than $10g$, but still within $15g$. In contrast, Figures 7a and 7b show that variation of prestress and damping cause the peak acceleration to vary by a factor of 10 or more for multi-stage prisms. Figure 7a shows that the two-stage prism can keep payload acceleration well below $10g$ for $\bar{\gamma} \in [10^{-3}, 10^{3}]$ N/m, i.e. for a large range of prestress, provided that the string damping is $c = 100$ N-s/m. According to Figure 7b, the three-stage prism can also achieve less than $10g$ acceleration for string damping $c = 500$ N-s/m and prestress parameter $\bar{\gamma} \in [100, 300]$ N-s/m.

Figures 8a and 8b show the equivalent results for two-stage and three-stage DHT landers respectively. Unlike the prism landers, none of the combinations of prestress and damping used for the simulation can achieve the *preferred* acceleration bound of $10g$. However, some combinations are still seen to achieve the *required* bound of $20g$. The combination $c = 1000$ N-s/m and $\bar{\gamma} \in [100, 300]$ N/m achieves payload acceleration within $20g$ for the two-stage DHT, while $c = 1000$ N-s/m, $\bar{\gamma} \in [100, 500]$ N/m achieves the same for the three-stage DHT.

Step II: Chosen Prestress and Damping; Reducing Bar Diameter and Comparing Mass and Acceleration

In the first step with bar diameters 8 cm, the single-stage prism, two-stage prism, three-stage prism, two-stage DHT, three-stage DHT have masses 41.3, 65.9, 91.9, 144.4, 203.4 kg respectively. The second step seeks to investigate if it is possible to reduce mass without failing the structure, and still achieve acceleration within the preferred bound of $10g$. To this end, the combination of damping and prestress leading to the lowest payload acceleration in step I is selected for each architecture. The bar diameter is progressively reduced until one of two things happen: (a) payload acceleration exceeds $10g$ ($20g$ may be allowed for DHT landers), (b) the load in a member exceeds 50% of the failure load (yielding for strings, minimum of yielding and buckling for bars). For simplicity of design, the diameter of every bar is reduced by the same amount simultaneously. Once the minimum possible bar diameter is reached, the prestress parameter $\bar{\gamma}$ is varied to see if the acceleration can still be reduced further. Following this procedure, Table 1 gives the minimal mass candidate for each of the five lander architectures.

Lander architecture	String damping (N-s/m)	Prestress parameter (N/m)	Bar diameter (cm)	Structure mass (kg)	Peak payload acceleration (earth-g)
Single-stage prism	1000	0.1	2	2.9	6.6
Two-stage prism	100	10	1.5	2.7	5.3
Three-stage prism	10	300	2	6.3	4.4
Two-stage DHT	1000	100	4	37.3	13.0*
Three-stage DHT	1000	100	4	52.5	17.3*

Table 1: Minimal mass candidates for the five lander architectures
(*some bars are on the verge of buckling for DHT landers)

Table 1 shows a clear advantage of using the tensegrity prism over DHT to construct the lander. The prism landers need less mass and lead to less acceleration of the payload compared to the DHT landers. At the same time, the prism landers have a good margin of safety in terms of failure by yielding or buckling, in the sense that the maximum load in a member is always less than 50% of what will cause it to fail. Among the three prism landers, the two-stage prism architecture has the lowest mass and an acceptable value of the peak acceleration.

CONCLUSIONS AND FUTURE WORK

This paper investigated a total of five different lander architectures designed using two well-known tensegrity topologies and making appropriate modifications. A trade study established a range of prestress and damping which ensured the peak acceleration of the payload less than 10 times earth gravity for the prism landers, and 20 times earth gravity for the DHT landers. Candidate minimal mass designs were obtained by reducing the bar diameters. Compared to the DHT landers, the prism landers needed less mass, led to a smaller acceleration of the payload, and were safer in terms of keeping the bars and strings intact. Although the mass and acceleration values were close for the single-stage, two-stage, and three-stage prism landers, the two-stage version required the minimum mass, and yet produced acceptable acceleration.

Future work will be carried out in two directions. First, a more systematic procedure to find out the minimal mass design for the dynamic simulations will be investigated. Second, the best architecture from this study will be compared with other existing tensegrity lander topologies.

ACKNOWLEDGEMENT

Some of the work in this paper is partially supported by the National Science Foundation under Award No. NSF CMMI-1634590 and by Texas A&M University.

REFERENCES

Bel Hadj Ali, N., S. I. (2010). "Dynamic behavior and vibration control of a tensegrity structure." *International Journal of Solids and Structures*, 47, 1285–1296.

Carpentieri, G., Skelton, R. E., and Fraternali, F. (2015). "Minimum mass and optimal complexity of planar tensegrity bridges." *International Journal of Space Structures*, 30(3-4), 221–243.

Fuller, R., Applewhite, E., and Loeb, A. (1975). *Synergetics; explorations in the geometry of thinking*. Macmillan.

Goyal, R., Chen, M., Majji, M., and Skelton, R. E. (2019a). "Motes: Modeling of tensegrity structures." *Journal of Open Source Software*, 4(42), 1613.

Goyal, R., Peraza Hernandez, E. A., and Skelton, R. (2019b). "Analytical study of tensegrity lattices for mass-efficient mechanical energy absorption." *International Journal of Space Structures*, 34(1-2), 3–21.

Goyal, R. and Skelton, R. E. (2019). "Joint optimization of plant, controller, and sensor/actuator design." *2019 American Control Conference (ACC)*, 1507–1512 (July).

Goyal, R. and Skelton, R. E. (2019). "Tensegrity system dynamics with rigid bars and massive strings." *Multibody System Dynamics*, 46(3), 203–228.

Karnan, H., Goyal, R., Majji, M., Skelton, R. E., and Singla, P. (2017). "Visual feedback control of tensegrity robotic systems." *2017 IEEE/RSJ-IROS*, 2048–2053.

Li, F., de Oliveira, M. C., and Skelton, R. E. (2008). "Integrating Information Architecture and Control or Estimation Design." *SICE Journal of Control, Measurement, and System Integration*, Vol.1(No.2).

Nagase, K. and Skelton, R. E. (2014). "Double-helix tensegrity structures." *AIAA Journal*, 53(4), 847–862.

Paul, C., Valero-Cuevas, F. J., and Lipson, H. (2006). "Design and control of tensegrity robots for locomotion." *IEEE Transactions on Robotics*, 22(5), 944–957.

Rimoli, J. J. (2016). "On the impact tolerance of tensegrity-based planetary landers." *57th AIAA/ASCE/AHS/ASC Structures, Structural Dynamics, and Materials Conference, AIAA SciTech Forum*, 1511 (8 Pages).

Skelton, R. and de Oliveira, M. (2009). *Tensegrity Systems*. Springer US.

Skelton, R. E. and de Oliveira, M. C. (2010a). "Optimal complexity of deployable compressive structures." *Journal of the Franklin Institute*, 347(1), 228–256.

Skelton, R. E. and de Oliveira, M. C. (2010b). "Optimal tensegrity structures in bending: the discrete Michell truss." *Journal of the Franklin Institute*, 347(1), 257–283.

SunSpiral, V., Gorospe, G., Bruce, J., Iscen, A., Korbel, G., Milam, S., Agogino, A., and Atkinson, D. (2013). "Tensegrity based probes for planetary exploration: Entry, descent and landing (edl) and surface mobility analysis." *International Journal of Planetary Probes*, 7 (13 Pages).

Sutton, G. H. and Duennebier, F. K. (1970). "Elastic properties of the lunar surface from surveyor spacecraft data." *Journal of Geophysical Research*, 75(35), 7439–7444.

Tibert, A. G. and Pellegrino, S. (2003). "Deployable tensegrity mast." *In: 44th AIAA/ASME/ASCE/AHS/ASC, Structures, Structural Dynamics and Materials Conference and Exhibit, Norfolk , VA, USA.*, 1978.